ATMOSPHERIC AEROSOL PROPERTIES

EFFECT OF VOLCANIC AEROSOL ON

ATMOSPHERIC AEROSOL PROPERTIES

by

RONALD SCHROEDER

A Thesis

Submitted to the Department of Geography

in Partial Fulfillment of the Requirements

for the Degree

Bachelor of Arts

McMaster University

April 1984

BACHELOR OF ARTS (1984) McMASTER UNIVERSITY

(GEOGRAPHY) Hamilton, Ontario

TITLE: Effect of Volcanic Aerosol on Atmospheric Aerosol Properties

AUTHOR: Ronald Schroeder

SUPERVISOR: Dr. J.A. Davies

NUMBER OF PAGES: ix, 42

ABSTRACT

Aerosol particle size and mass were estimated from spectral aerosol optical depths. Optical depths were calculated from sunphotometer measurements before and after the eruption of El Chichón in 1982. Although aerosol parameters varied considerably with synoptic conditions, an increase in aerosol size and mass after the eruption was evident.

ACKNOWLEDGEMENTS

I greatly appreciate the support, humour, criticism and guidance of my supervisor, Dr. J.A. Davies. I also wish to thank Dr. L.J.B. McArthur for his patience in answering my questions, for debugging my programs, and for his suggestions. Thanks are also extended to Kathleen Stewart for providing the 1981 data set, to Archibald Ashbridge providing ozone data, and to Heidi Maskell, my typist.

The study is funded by the National Science and Engineering Research Council of Canada, and the Atmospheric Environmental Service.

TABLE OF CONTENTS

LIST OF FIGURES

LIST OF TABLES

LIST OF SYMBOLS

a, b, c	coefficients for Deirmendjian aerosol size distribution
ab	absorption
ext	extinction
m	optical air mass
$n_c(r)$	columnar number size disbribution
r	geometric aerosol cross-section
r_m	aerosol mode radius
sc	scattering
$\bar{r}/r$	ratio of mean to actual earth-sun distance
C	optical cross-section
I	incident radiation at the surface
I_o	mean extraterrestrial radiation
I_o'	extraterrestrial radiation adjusted for earth-sun distance
I_d	diffuse radiation
M_c	mass loading
N	number of particles
Q	Mie efficiency factor
V	mean calibration constant
V_o'	calibration constant adjusted for earth-sun distance
V_c	columnar aerosol volume
α, β	coefficients of power law
α_o, β_o	theoretical α and β used in inversion process

γ, ε	empirical parameters for Deirmendjian distribution
λ	wavelength
η	refractive index
ρ	particle density
τ	optical depth
τ_a	aerosol optical depth
τ_R	rayleigh optical depth
τ_{oz}	ozone optical depth
τ_w	water optical depth
τ_x	other optical depth

CHAPTER ONE

INTRODUCTION

Because aerosols* attenuate radiation by absorption and backscattering, they have the potential to modify climate. The process of attenuation depends on the number, size, and refractive index of the aerosol particles. There are few studies of aerosol physical properties in the field of climatology.

It has been established that backscattering due to an increase in stratospheric aerosol, following volcanism, produces surface cooling. This was observed following the Mt. Agung (Bali) eruption in 1963 (Pollack et al. 1976). The recent major eruption of El Chichón, Mexico (17.33^{o}N, 93.2^{o}W) in the spring of 1982 provides an opportunity to study the effect of volcanism on stratospheric aerosol, radiation and climate. El Chichón produced 40 times more stratospheric aerosol than the eruption of Mount St. Helens, and is the most massive aerosol cloud of the last 100 years. (Pollack et al. 1983; Hofmann and Rosen 1983).

The variation in tropospheric aerosol properties are more complex since they emanate from different sources. Major sources are sea salts, combustion (both natural and man-made), and windblown dust (Prospero et al. 1983). Characteristics of aerosols vary both

---

*suspended solids and liquids, excluding water, in the atmosphere.

spatially and temporally. At a given location, synoptic air mass trajectories can indicate possible origins for imported aerosol. Wind direction is a rough indicator of air mass trajectories. Wind speed is also an important factor in explaining variation in aerosol. High wind speed disperses local aerosol and may increase the amount of windblown dust. High relative humidity changes the size and shape of hygroscopic particles by providing water (Hänel 1976; Paltridge and Platt 1976). Meteorological conditions are important in the explanation of aerosol variations.

In this study, a method presented by Box and Lo (1976) is used to determine particle size distribution parameters from calculated attenuation, using measured spectral solar radiation. This method has been previously applied by Russell, Livingston, and Uthe (1979) but only for a duration of six hours. The results of the Box and Lo analysis are used to calculate the aerosol mass loading and mode radius of the aerosol size distributions. Spectral radiation measurements were obtained during periods when direct solar radiation was unobstructed by cloud during 1981 and 1983. Most of the data was obtained during late spring and summer. Variability in aerosol mass loading and mode radius is examined to show effects of El Chichón and synoptic conditions.

CHAPTER TWO

THEORETICAL BACKGROUND

Determination of aerosol mass loading and mode radius from sunphotometer measurements is based on radiative transfer principles and an approximation of particle size distributions.

Assuming that aerosol particles are spherical, the geometric cross-section of a particle of radius r is πr^2. Its optical cross-section C for absorption ab and scattering sc (van de Hulst 1957) is the area normal to an incident wave that intercepts the same amount of energy that a particle absorbs or scatters. The optical cross-section for both scattering and absorption C_{ext} is defined as

$$C_{ext} = C_a + C_{sc} \tag{1}$$

Optical cross-sections are a function of the radius, the wavelength λ of the incident radiation, and the refractive index η of the particle. The refractive index governs the particles' ability to scatter and absorb. The ratio of the optical and geometric cross-sections is the Mie efficiency factor Q_{ext}. For extinction

$$Q_{ext}(\lambda, r, \eta) = \frac{C_{ext}(\lambda, r, \eta)}{\pi r^2} \tag{2}$$

The aerosol optical depth $\tau_a(\lambda)$ is determined by integrating the optical cross-section over the number of particles in the column $n_c(r)$ for each radius.

$$\tau_a(\lambda) = \int_0^\infty Q_{ext}(\lambda, r, \eta)\pi r^2 n_c(r)dr \tag{3}$$

Deirmendjian (1969) has provided an analytical function for the aerosol size distribution n(r)

$$n(r) = c\ r^{\varepsilon} \exp(-br^{\gamma})\ \{cm^2 \mu m^{-1}\} \tag{4}$$

where c and b are fitted to experimental data

and ε and γ are empirical parameteres determined by Deirmendjian

Deirmendjian (1976) established that ε and γ are 2 and ½ respectively for continental type aerosol distributions (HazeL model). Kuriyan and Sekara (1974) and Kuriyan et al. (1974) find that Deirmendjian's high-level, or stratospheric model (HazeH) having ε and γ set to 2 and 1 respectively, reproduce the scattering properties of the HazeL model, and therefore conclude that only the HazeH model is required.

Using the HazeH distribution, the total number of particles N is determined by integrating over all radii. Thus

$$N = c\int_0^\infty r^2\ e^{-br}dr \tag{5}$$

$$= 2\ c/b^3$$

since $c = \frac{1}{2}\ ab^3$

$$n_c(r) = \tfrac{1}{2}\ ab^3\ r^2\ e^{-br} \tag{6}$$

Box and Lo (1976) provide a method for determining a and b in equation (6). Equation (3), and the empirical relationship between $\tau_a(\lambda)$ and λ,

$$\tau_a(\lambda) = \beta(\lambda/\lambda_0)^{-\alpha} \tag{7}$$

where $\lambda_0 = 1\ \mu m$ (Ångström 1964)

are used in the method.

Theoretical values of optical depth $\tau_a(\lambda)_o$ are calculated for a range of b values. a in equation (6) is set to equal 1, and $\tau_a(\lambda)_o$ determined by equation (3). The Mie scattering computations assume a typical urban refractive index of $1.5 - 0.1_i$.

Using $\tau_a(\lambda)_o$, theoretical values of β_o and α_o are determined from equation (7) by a least squares method. Equating α and α_o, b is obtained from a graph of α as a function of b (Figure 1). Since

$$a = \frac{\beta}{\beta_o} \tag{8}$$

and β_o^{-1} is determined from a graph of b versus β_o^{-1} (Figure 2), a is easily determined.

Actual values of α and β in equation (7) are determined by a non-linear least squares using $\tau_a(\lambda)$ value from spectral radiation measurements.

Values of $\tau_a(\lambda)$ are obtained from Beer's Law, which states that

Figure 1. Relationship between α and b HazeH model

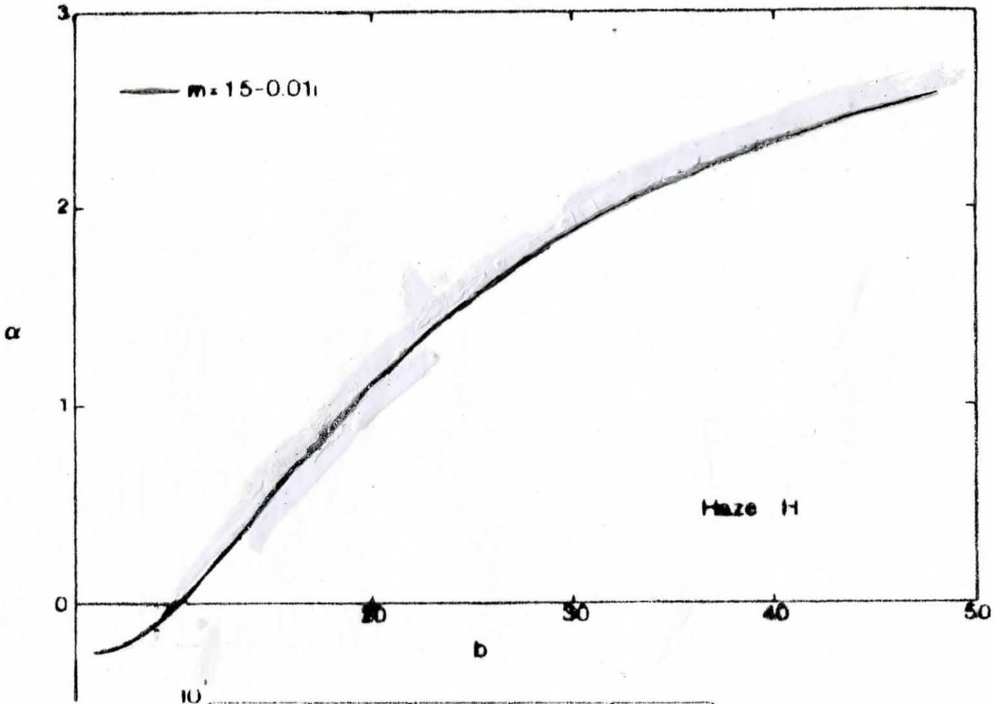

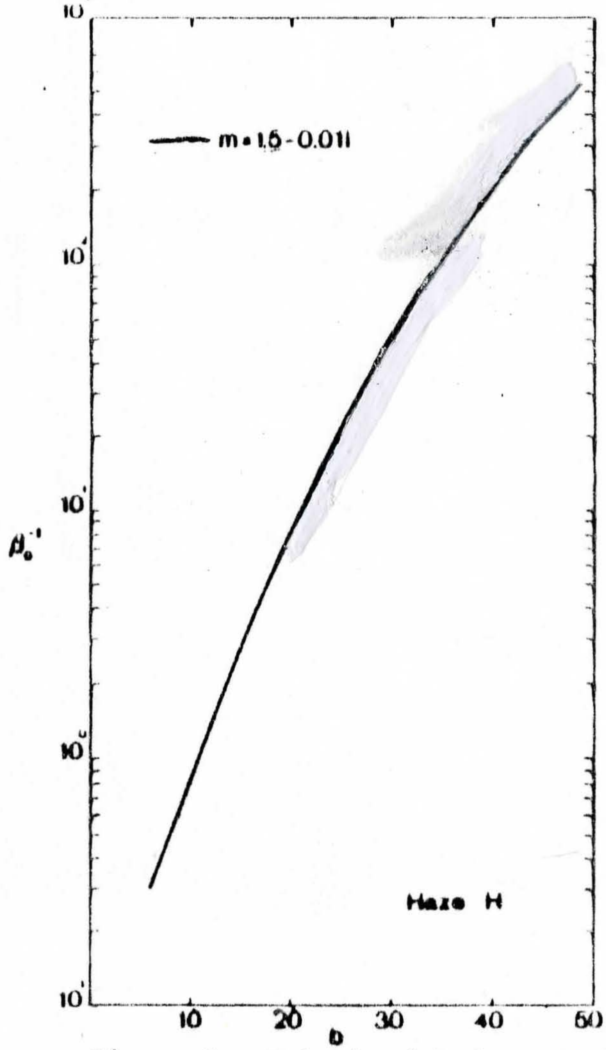

Figure 2. Relationship between b and β_o^{-1} HazeH model

$$I(\lambda) = (\frac{\bar{r}}{r})^2 \, I_o(\lambda) \, \exp\,(-\tau_t(\lambda)m) + I_d(\lambda) \qquad (9)$$

where $I(\lambda)$ is the incident radiation at the surface for wavelength (λ)

$(\frac{\bar{r}}{r})^2$ is the ratio of mean to actual earth-sun distance

$I_o(\lambda)$ is the mean extraterrestrial radiation for wavelength (λ)

$\tau_t(\lambda)$ is the total optical depth for wavelength (λ)

m is the optical air mass

and $I_d(\lambda)$ is the diffuse radiation received for wavelength (λ)

(Stewart 1981)

Given a sunphotometer viewing angle of 3^o or less, and a zenith angle of less than 80^o, $I_d(\lambda)$ contributes less than 2% of the total radiation, and is therefore ignored (Shaw, et al. 1973).

Rearranging equation (9)

$$\tau_t(\lambda) = m^{-1} \ln \frac{I(\lambda)}{I_o'(\lambda)} \qquad (10)$$

where $I_o'(\lambda)$ is the extraterrestrial radiation, adjusted for earth-sun distance, at wavelength (λ)

Since sunphotometer measurements provide voltages proportional to radiation intensities, equation (10) is rewritten as

$$\tau_t(\lambda) = m^{-1} \ln \frac{V(\lambda)}{V_o'(\lambda)} \qquad (11)$$

where $V(\lambda)$ and $V_o'(\lambda)$ are sunphotometer voltages corresponding to $I(\lambda)$ and $I_o'(\lambda)$

Because of variations in earth-sun distances

$$V_o'(\lambda) = \left(\frac{\bar{r}}{r}\right)^2 V_o(\lambda) \tag{12}$$

where $V_o(\lambda)$ is the extraterrestrial sunphotometer reading (calibration constant) for the mean earth-sun distance, for wavelength (λ)

The total optical depth $\tau_t(\lambda)$ equals the sum of each contributing component. Thus

$$\tau_t(\lambda) = \tau_a(\lambda) + \tau_R(\lambda) + \tau_{oz}(\lambda) + \tau_w(\lambda) + \tau_x(\lambda) \tag{13}$$

where $\tau_a(\lambda)$ is the aerosol optical depth at wavelength (λ)

$\tau_R(\lambda)$ is the rayleigh optical depth at wavelength (λ)

$\tau_{oz}(\lambda)$ is the ozone optical depth at wavelength (λ)

$\tau_w(\lambda)$ is the water vapour optical depth at wavelength (λ)

and $\tau_x(\lambda)$ are other optical depths at wavelength (λ)

$\tau_a(\lambda)$ is calculated by subtracting other components from the total optical depth. Usually wavelengths are selected where the water vapour component is zero, thereby simplifying the equation.

Using measured $\tau_a(\lambda)$ values to determine α and β , the Box and Lo method was used to determine a and b for Deirmendjian's (1969) number-size distributions. Using the HazeH model of equation (6), the volume $V_c(m^3\ m^{-2})$ is determined through integration.

$$V_c = \frac{4}{3}\pi\int_0^\infty \tfrac{1}{2}\ ab^3\ r^5\ e^{-br}\ dr \tag{14}$$

The solution to the integral is $120/b^6$ (Gradshteyn and Ryzhnik, 1965). Assuming a particle density ρ(mg cm^{-3}) the mass loading (M_c) is

$$M_c = 80\rho\,\pi\, ab^{-3} \ (\mathrm{mg\ m^{-2}}) \tag{15}$$

Similarly the mode radius r_m of the distribution is determined through differentiation. Thus

$$r_m = 2/b\ (\mu\mathrm{m}) \tag{16}$$

Values for a and b are obtained for Deirmendjian's HazeL model (Figures 3 and 4) using a similar analysis (Davies, et al. 1984). For the HazeL model

$$M_c = 443520\ \rho\,\pi\, ab^{-6} \ (\mathrm{mg\ m^{-2}}) \tag{17}$$

and $$r_m = 16/b\ \ (\mu\mathrm{m}) \tag{18}$$

Comparisons of the two models are made later.

Figure 3. Relationship between α and b HazeL model

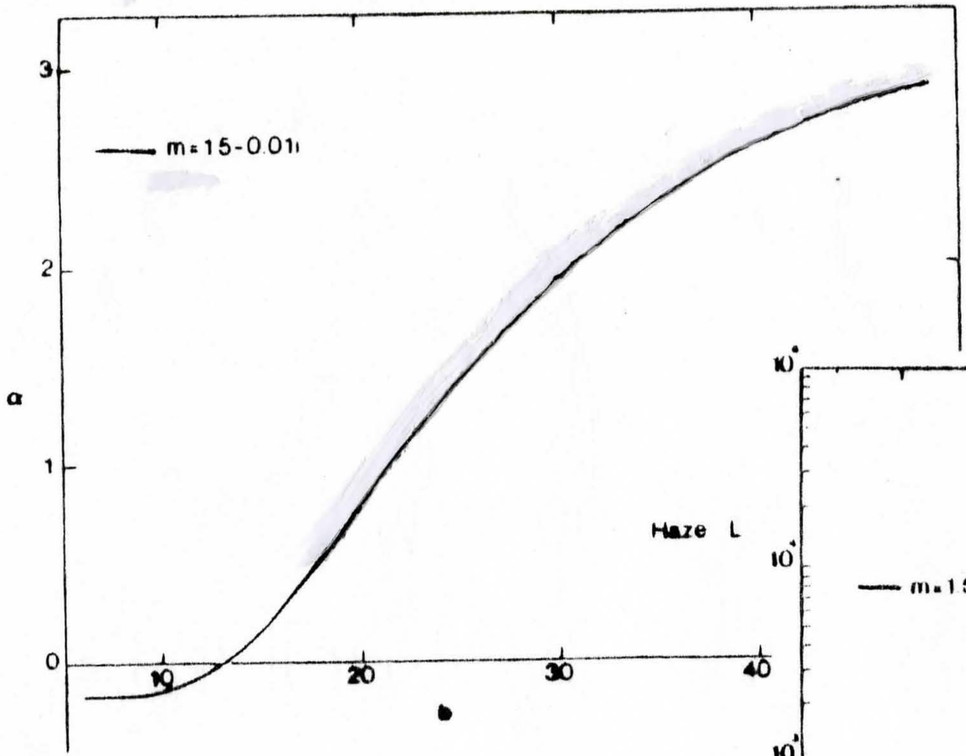

Figure 4. Relationship between b and β_o^{-1} HazeL model

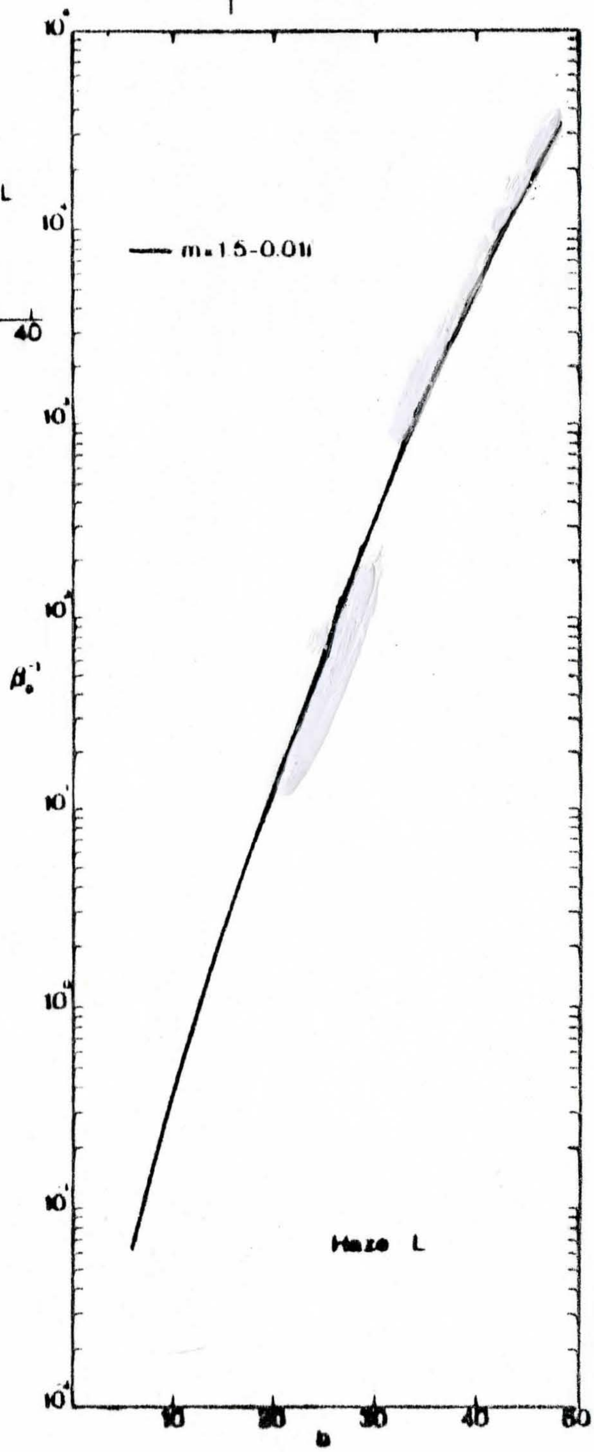

CHAPTER THREE

EXPERIMENTAL BACKGROUND

Rooftop sunphotometer measurements of direct beam solar radiation were made for 9 wavelengths at McMaster University, Hamilton, Ontario ($43^{\circ}15'41''$, $79^{\circ}55'19''$). Measurements were taken at approximately 15 to 20 minute intervals during cloud free times and required a timespan of approximately 2 minutes to complete. The measurement program ran from March 1981 to August 1981, and again from January 1983 to September 1983.

The sunphotometer (Figure 5) was built at the University of Arizona, and is similar to one described by Shaw, et al. (1973). A collimating tube defines a 3° field of view and accurate sighting of the sun was achieved with a peep-hole sight. Narrow band ($\sim$ 100 Å) interference filters were mounted in a filter wheel and were centred on the following wavelengths: .4000, .4385, .5000, .5200, .6100, .6700, .7800, .8690, and 1.0285 μm. 100 Å bandwidths are sufficiently narrow to ensure an error of less than .1% for wavelengths greater than .45 μm (Thomason, et al., 1982).

Radiation was detected by a temperature sensitive photodiode, (EG and G UV-44B). Calibrations were determined in 1980 with a photodiode temperature of $31.5^{\circ}C$. Although photodiode temperatures reached $40^{\circ}C$ in the 1981 measuring period, recalibrations in 1982 with a photodiode temperature of $40^{\circ}C$ showed little difference in calibration constants,

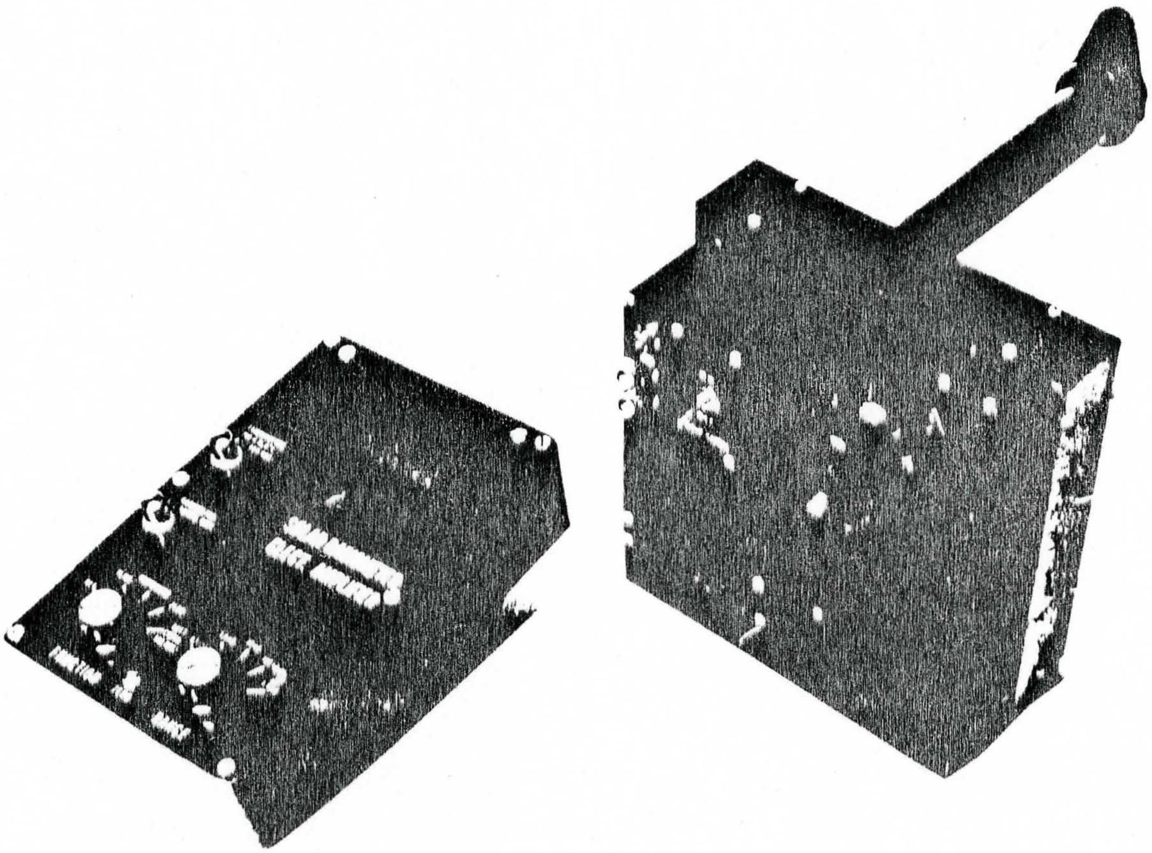

Figure 5. The sunphotometer and amplifier.

Figure 5. The sunphotometer and amplifier.

and temperature dependence was ignored, (Davies 1982; Table 1). During the 1983 measurement period, 40°C photodiode temperatures were maintained by a heating circuit, and temperatures rarely departed by more than .2°C.

Calibration of the instruments was carried out by Professor Reagan in Tucson, Arizona on days with little diurnal variation in aerosol. The Langley plot method used consists of extrapolation of a plot of the logarithm of measured voltages, against airmass, to zero airmass. Calibration constants, and associated errors about the constants are listed in Table 1.

The sunphotometer is equipped with a digital voltmeter-amplifier which allows a greater sensitivity to be selected at low irradiances. The amplifier also displays battery voltage, photodiode temperature, and a zero-offset. Periodic checks of these were made to ensure that the instrument was operating properly.

From date, time and location, optical airmass and the ratio of mean to actual earth-sun distances were determined using equations given by Paltridge and Platt (1976). Although airmass can be calculated accurately, Table 2 shows that errors up to 10% with large zenith angles, may occur with a 2 minute error in time. Since few measurements were made with such large zenith angles, and since this error is common to all wavelengths, it was ignored.

Rayleigh optical depths were calculated by an equation derived by Fröhlich and Shaw (1980)

Table 1. Filter bandwidths, calibration constants and error about the constants, and ratio between calibrations taken in 1980 and 1982 for the nine wavelengths.

Wavelenght (Å)	Filter Bandwidth (Å)	Calibration Constants & Error			Stability in Calibration 1982/1980
		Instrument 1		Instrument 2	
		1980 T=31.5°C	1982 T=40.0°C	1982 T=40.0°C	
4000	90	218.3± 5.6	227.2± 2.3	204.8± 2.5	1.041
4385	75	332.5± 5.6	333.5± 2.1	400.4± 2.9	1.003
5000	74	560.6± 6.9	561.0± 1.0	649.2± 5.2	1.001
5200	82	740.9± 8.2	743.5±16.0	831.7±10.3	1.004
6100	103	998.2± 9.0	1023.8± 1.5	1091.6± 8.7	1.026
6700	108	1386.3±12.1	1384.2± 4.5	1296.2± 9.1	0.998
7800	110	920.0± 8.4	925.5± 3.3	894.2± 8.4	1.006
8690	122	959.6± 8.2	968.9± 4.6	1070.0± 9.8	1.010
10285	148	573.3± 1.9	618.4± 3.2	600.3± 8.7	1.067

Table 2. Error in Optical Air Mass as a result of a ±2 minute Error in Local Apparent Time. Air Mass calculated for a Solar Declination of 21.5° and a latitude of 43.255°

LAT	Air Mass ±2 minutes from LAT	% Difference
1200 1200	1.0759 1.0759	0
1700 1300	1.1051 1.1014	.34
1000 1400	1.1963 1.1879	.70
900 1500	1.3751 1.3595	1.13
800 1600	1.7056 1.6764	1.17
700 1700	2.3639 2.3021	2.61
600 1800	4.0125 3.8335	4.46
500 1900	12.2992 10.9100	11.30

$$\tau_R(\lambda) = \frac{P}{101.326} \; .00838\lambda^{-(3.9164 + .074\lambda + \frac{.05}{\lambda})} \qquad (19)$$

where P is the atmospheric pressure (kP_a)

A daily mean value of atmospheric pressure was calculated from barometric measurements taken approximately once every 4 hours. The Rayleigh scattering optical depth has an estimated accuracy of 3% (Russell, et al., 1979).

Values of ozone optical depths $\tau_{oz}(\lambda)$ were determined from

$$\tau_{oz}(\lambda) = a_o(\lambda) \; u_o \qquad (20)$$

where $a_o(\lambda)$ is the ozone absorption coefficients at wavelength (λ) Elterman (1968)

and u_o is the measured ozone content (atm -cm)

Ozone absorption coefficient values are given in Table 3. Daily ozone quantities were measured by the Atmospheric Environmental Service at Downsview, Ontario. Error in ozone optical depths was set as 15% (Russell, et al., 1979). Since ozone optical depths are very small, any error contributes little to the error in aerosol optical depths.

All filters were selected for wavelengths where water vapour does not absorb.

No account was taken of other absorbing gases. Shaw (1976) and Russell, et al. (1979) state that NO_2 absorption may be significant, but there is little evidence to support this opinion. Since no measurements of NO_2 concentrations throughout the atmosphere were available for the area, NO_2 effects were ignored.

Errors in calculated aerosol optical depth values were determined by the method of propagation of errors (Bevington, 1969):

$$\Delta\tau_a(\lambda)^2 = \frac{1}{m^2}\left(\frac{\Delta V_o(\lambda)^2}{V_o(\lambda)^2} + \frac{\Delta V(\lambda)^2}{V(\lambda)^2}\right) + (.03\ \tau_R(\lambda))^2 + (.15\ \tau_o(\lambda))^2 \quad (21)$$

where $\Delta V_o(\lambda)$ are the standard deviation values found in Table 1

and $\Delta V(\lambda)$ is the uncertainty in the instantaneous voltage and is set to 1%

Table 3. Ozone Absorption Coefficients (a_o) for Wavelength (λ)

λ (μm)	a_o
.4	0.0000
.44	.0079
.5	.0345
.52	.0501
.61	.1180
.67	.0464
.78	.0126
.87	.0031
1.03	0.0000

Alpha and beta values (equation 7) were determined using a Marquardt non-linear least squares method. Each aerosol optical depth was weighted by the inverse square of its measurement uncertainty, thereby ensuring that each data point contributed to the derived parameters only in proportion to its information content. Uncertainties

Table 4

$b = 30$	$\beta_o^{-1} = 50$	
$b = 30 \pm 2$ $\Delta b \rightarrow 32$ $\Delta b \rightarrow 28$	$\Delta\beta_o^{-1} \rightarrow 69$ $\Delta\beta_o^{-1} \rightarrow 36$	$\Delta\beta_o^{-1}/\beta_o$ .38 .28
$b = 30 \pm 3$ $\Delta b \rightarrow 33$ $\Delta b \rightarrow 27$	$\Delta\beta_o^{-1} \rightarrow 80$ $\Delta\beta_o^{-1} \rightarrow 31$	.60 .38

Effect on β_o^{-1} with small changes in b in alpha and beta were derived from the Marquardt method, and reflect the uncertainties in measured aerosol optical depths (Bevington 1969). Tests for fitness were also examined. These show that a good relationship exists between aerosol optical depths and their wavelengths.

The parameters a and b and their uncertainties, were determined from cubic spline relationships between α and b, and b and β_o^{-1} as shown, Figures 1 and 2 for the HazeH model, and Figures 3 and 4 for HazeL. Uncertainties in a and b are calculated by the same procedure using $\Delta\alpha$ and $\Delta\beta$. The uncertainty in mode radius is

$$\Delta r_m = 2/\Delta b \tag{22}$$

for the HazeH model. The error in mass loading is a function of a and b.

Since Δb, calculated from $\Delta\alpha$, was used to determine $\Delta\beta_o^{-1}$, and $\Delta\beta_o^{-1}$ and $\Delta\beta$ determined Δa, large errors in the mass loading were found. $\Delta\beta_o^{-1}$ was extremely sensitive to small changes in b (Table 4). The root mean square error in mass loading was estimated from

$$\frac{\Delta M_c}{M_c} = \{(\frac{\Delta\beta}{\beta})^2 + (\frac{\Delta\beta_o^{-1}}{\beta_o^{-1}})^2 - (\frac{3\Delta b}{b})^2\}^{\frac{1}{2}} \tag{23}$$

The particle density is unknown and was set to 1 g m^{-3}. Values may be as large as 2 g m^{-3}.

Hourly meteorological data used in the results were observed at the Hamilton weather office. Relative humidity was calculated from water vapour equations derived by Buck (1981).

CHAPTER FOUR

RESULTS

Approximately 600 observations were made in 1981, and 1200 in 1983. More date were available in summer and for morning hours because cloud was less frequent. During 1981, observations were taken between 0800 and 1700 hours. In 1983 observations were made from sunrise to sunset when possible. Approximately 20 days had observations throughout the day.

Mass loading results are about 15% larger for the HazeL than HazeH models (Figure 6). Although the mode radius values from the two models are well correlated, HazeH results are 2 to 4 times larger than HazeL results (Figure 7). The model number size distributions (Deirmendjian, 1969) suggest a shift to smaller modes for the HazeL model. Other work (Laulainen et al., 1978; DeLuisi et al., 1983; Hofmann and Rosen, 1983) has estimated the mode radius at around 0.2 μm. Since the HazeH model produces results closer to the mode radius of 0.2 μm, it is used in this thesis.

Comparison of aerosol optical depths before and after the El Chichón eruption (Figure 8) shows a mode frequency increase of approximately 0.1 at all wavelengths after the eruptions. Observations with optical depths greater than 0.5 in the .67 μm wavelength were omitted for all wavelengths because these high pollution days were unusual, and not comparable to the 1981 data set. The 0.1 shift across all wavelengths indicates that light attenuation, resulting

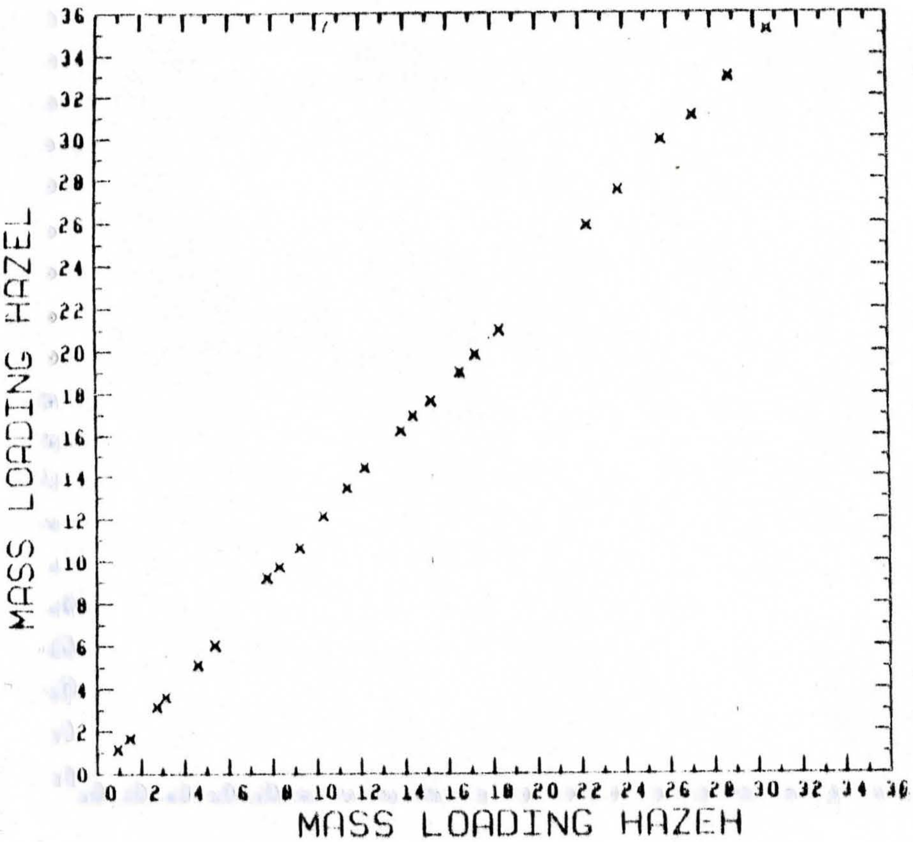

Figure 6. Comparison of Mass Loading for HazeH and HazeL models.

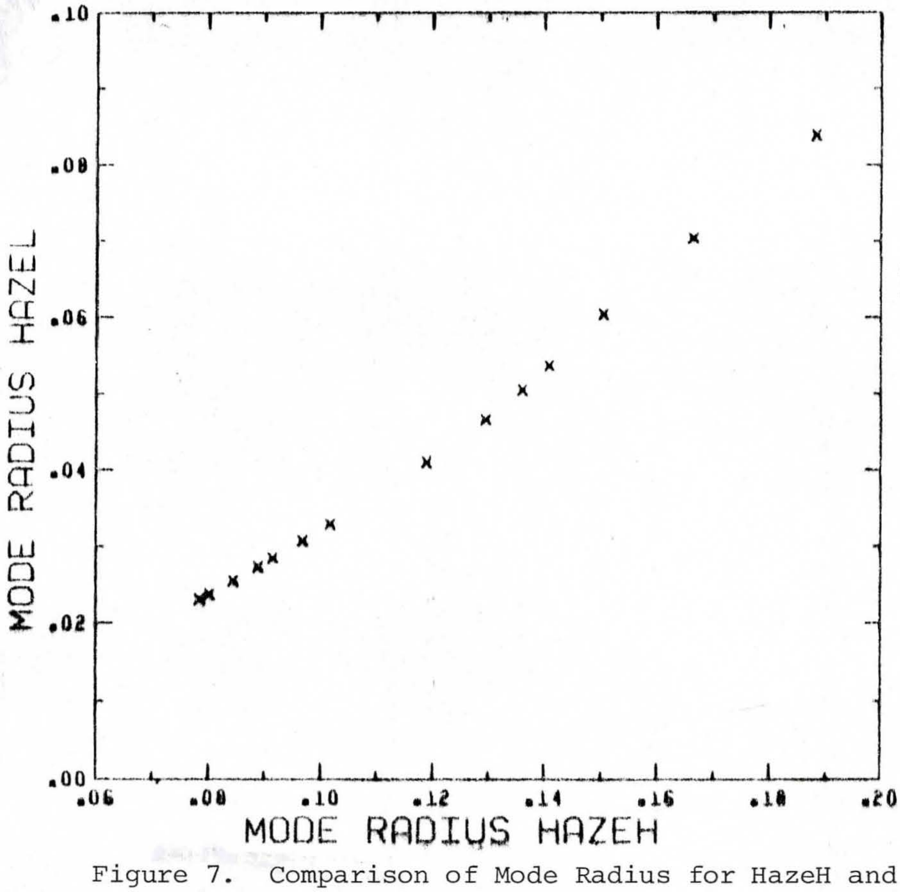

Figure 7. Comparison of Mode Radius for HazeH and HazeL models.

Figure 8. Frequency Distribution of spectral optical depths in 1981 and 1983

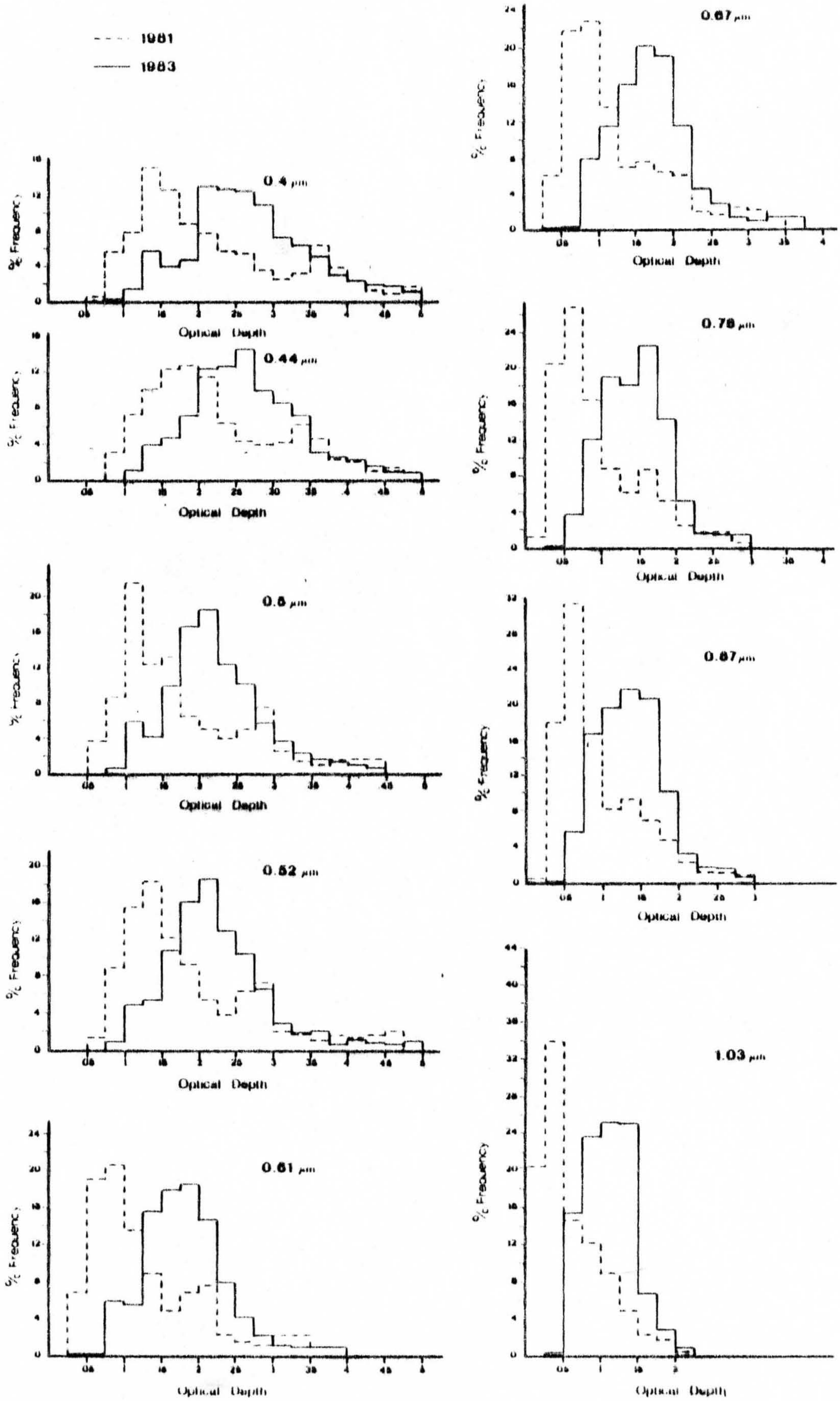

from the El Chichón eruption, is independent of wavelength.

Background stratospheric aerosol optical depths are very small (~ .005) (Pollack et al., 1976). Stratospheric aerosol optical depths, measured from airborne instruments, range between 0.08 and 0.1 (Spinhirne, 1983; Dutton and DeLuisi, 1983) for this latitudinal zone following the eruption. Little wavelength dependence for aerosol optical depths was found in either case (Figure 9).

Aerosol optical depths which are independent of wavelength indicate the presence of newly generated aerosols (DeLuisi et al., 1983). The resulting increase in aerosol optical depths of longer wavelengths, relative to the shorter wavelengths, indicates a presence of larger aerosol particles (Spinhirne, 1983).

Statistically significant increases, using Kolmogorov-Smirnov tests, have been found for the aerosol mode radius (Figure 10) and mass loading (Figure 11) from 1981 to 1983. Heavy pollution days in 1983 were omitted, as described earlier.

The frequency distribution of mode radii in 1983 was bimodal (Figure 11). Two distinct populations of radii are found, one before, and one after May, 1983 (Figure 12). Particle sizes and mass loading were expected to increase in the summer (Peterson et al., 1981; Figures 12 and 13, 1981). In June 1983, large winter radii decreased suddenly to values similar to those found in 1981. The mass loading decreased throughout 1983, but usually remained higher than 1981 values (Figure 13). Precipitation of larger particles, and continuing gas to particle conversion may explain why mode radius decreases, but mass loading levels remain relatively steady.

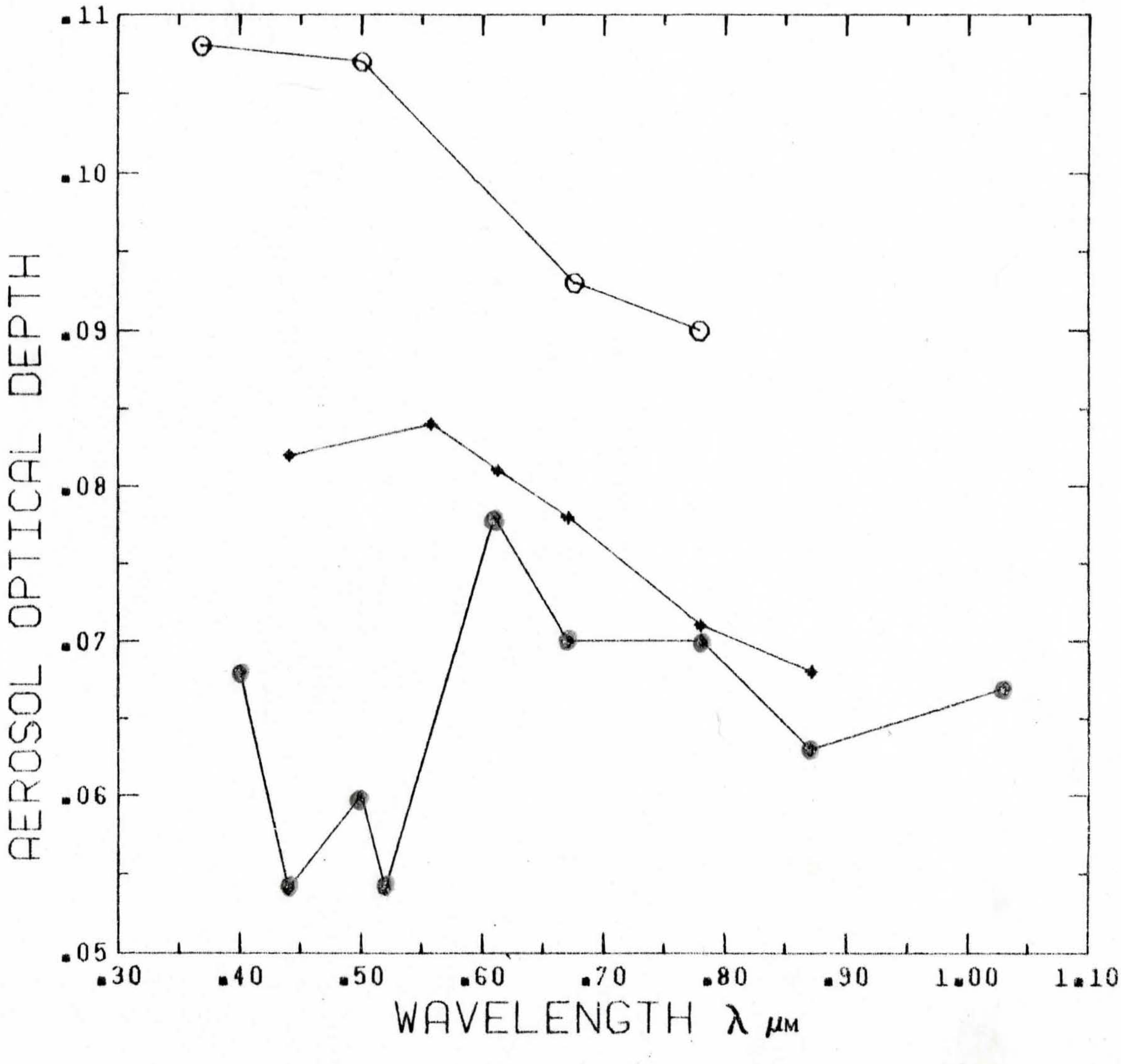

Figure 9. Variation of stratospheric aerosol optical depth with wavelength: (1) from ground-based measurements at Hamilton (●); (2) from ariborne measurements of Dutton and DeLuisi (○); (3) from airborne measurements of Spinhirne (∗).

Figure 10. Frequency distribution of aerosol mass loading in 1981 and 1983.

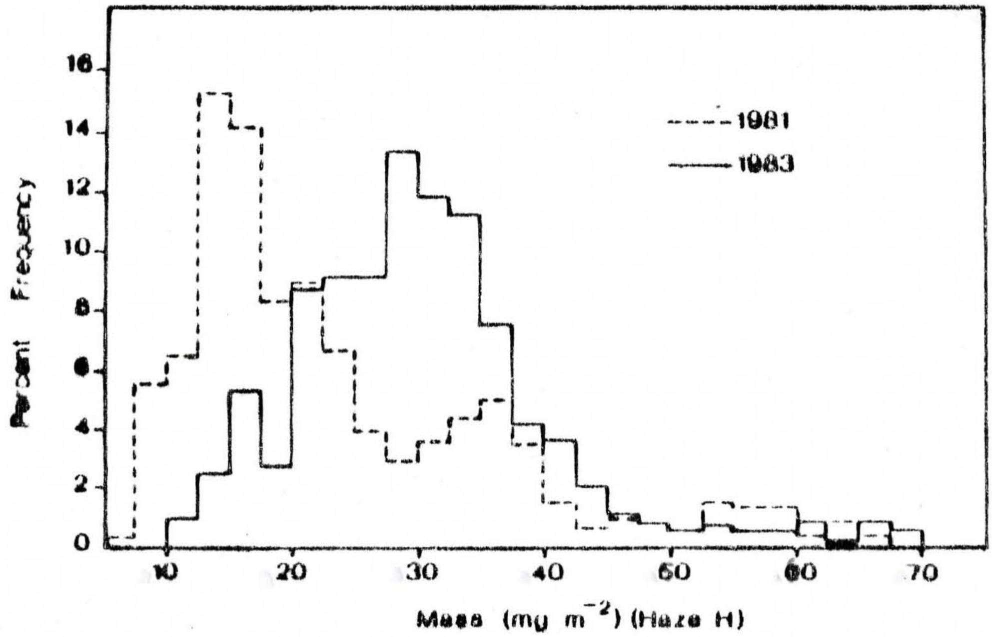

Figure 11. Frequency distribution of aerosol mode radius in 1981 and 1983.

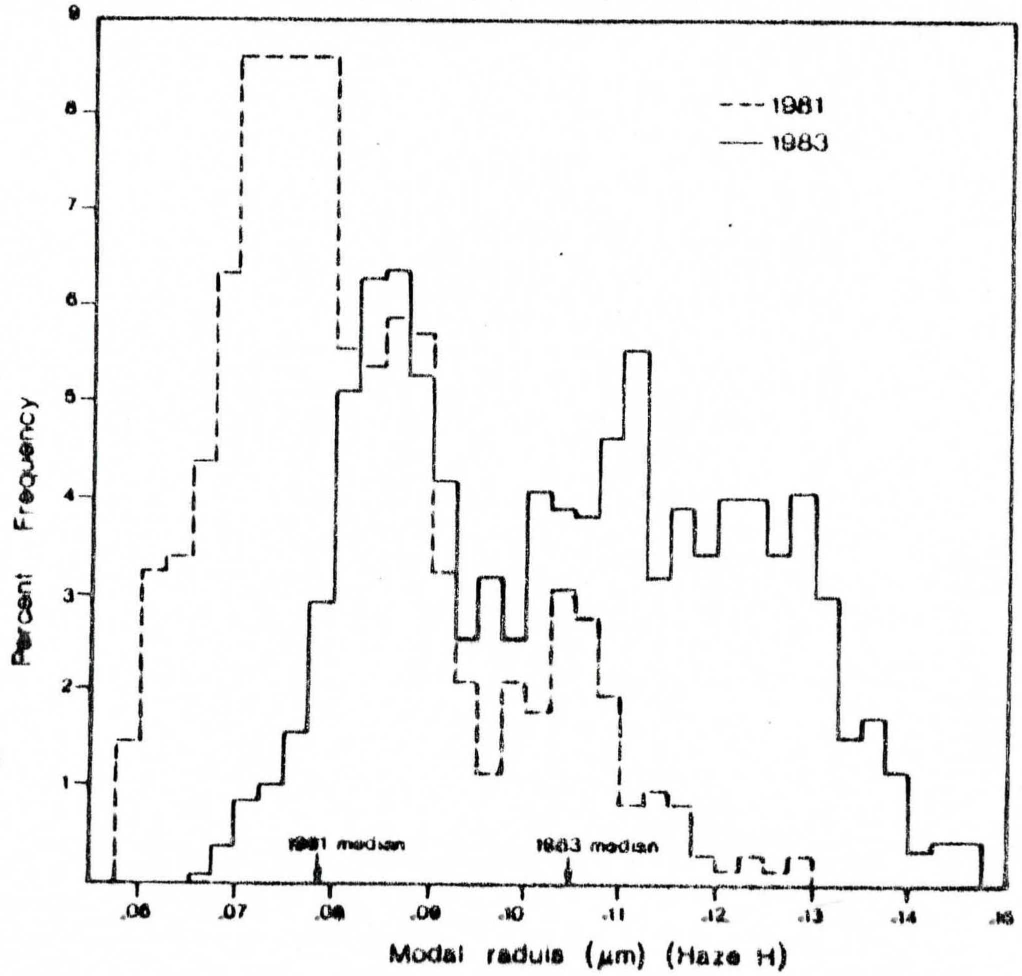

Figure 12. Monthly variation of median mode radius, with quartiles.

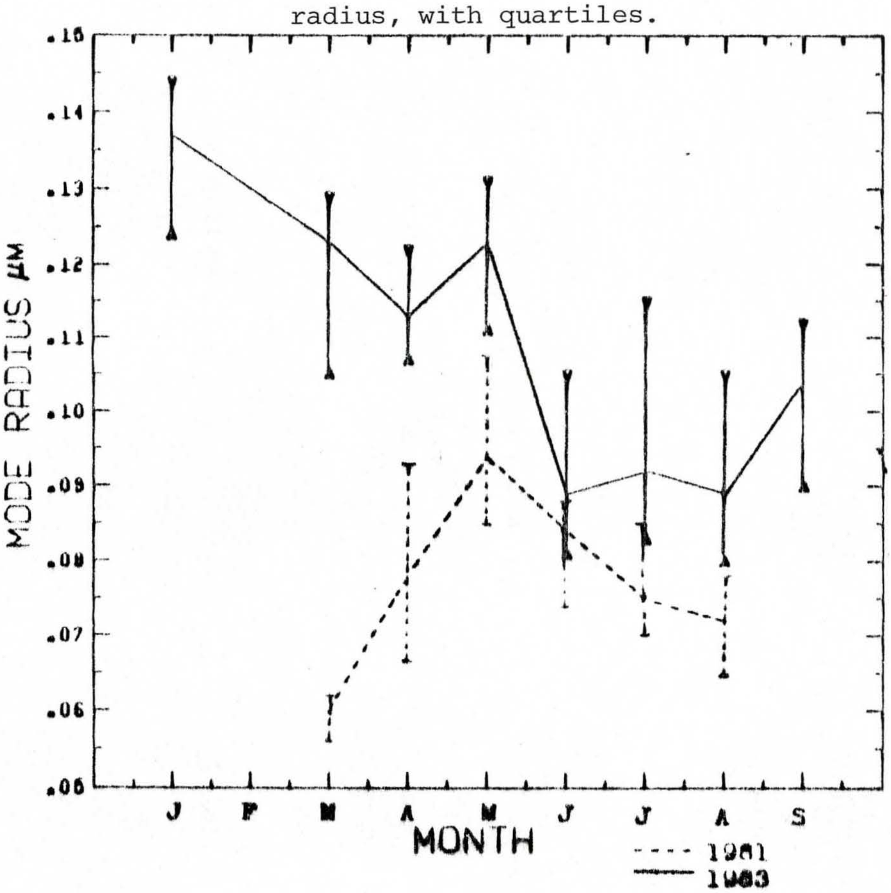

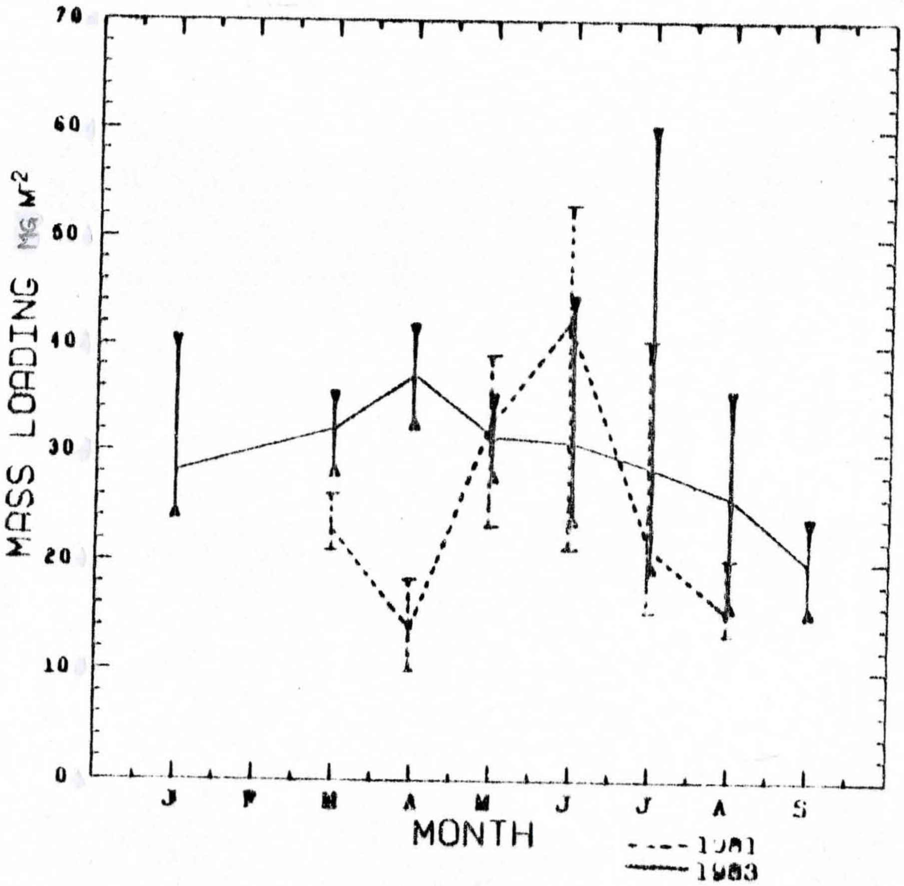

Figure 13. Monthly variation of median mass loading, with quartiles.

It has been found that visibility varies inversely with optical depths, and mass loading (Noll et al., 1968; Griffing, 1979; Kaufman and Fraser, 1983). Visibility is only determined by tropospheric conditions. No inverse relationship was found with visibility and mode radius or mass loading in either year (Figures 14 and 15). Similar results were found for 1981 and 1983 with visibilities less than 10 km. During clear days, with high visibilities, stratospheric effects are dominant, and both the mass loading and mode radius are larger in 1983 (Figures 14 and 15). It can be concluded that the stratospheric aerosol increases the mass loading and mode radius values in 1983.

Wind direction can influence turbidity (Peterson et al., 1981; Stewart, 1983). Relatively few observations with wind direction from the south-east exist (Figure 16). The mode radius during 1981 was largest with south-east winds (Figure 17). In 1983, much larger mode radii were found, and the maximum occurred with wind directions between west and north. North-west surface winds generally occur with a northern synoptic airmass. The relatively aerosol-free troposphere under such conditions emphasises the larger particles in the stratosphere. The mass loading was largest with south-east winds in 1981, and with south-west winds in 1983 (Figure 18). Minima occurred between north-west and north in both years, suggesting lighter aerosol levels in a northern airmass.

Hänel (1967) has shown experimentally that particles increase in size with a relative humidity greater than 60%. Correlations between optical depths and relative humidity have been found previously

Figure 14. Correlation between visibility and mode radius, • indicate median mode radius, Quartiles indicated by horizontal bars.

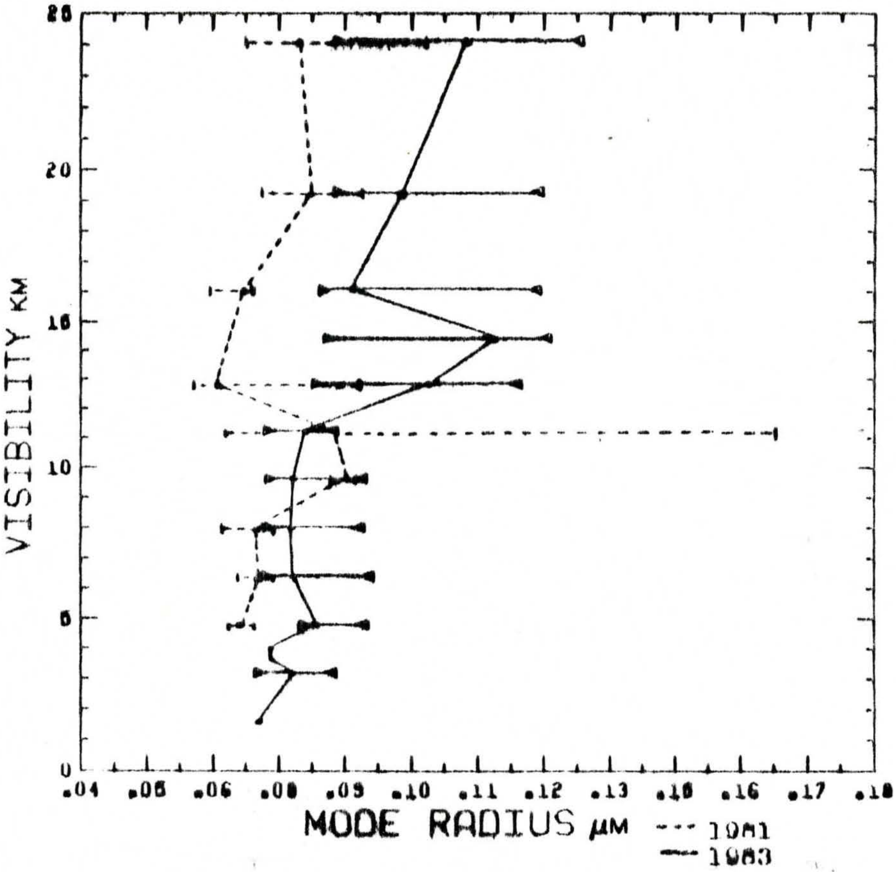

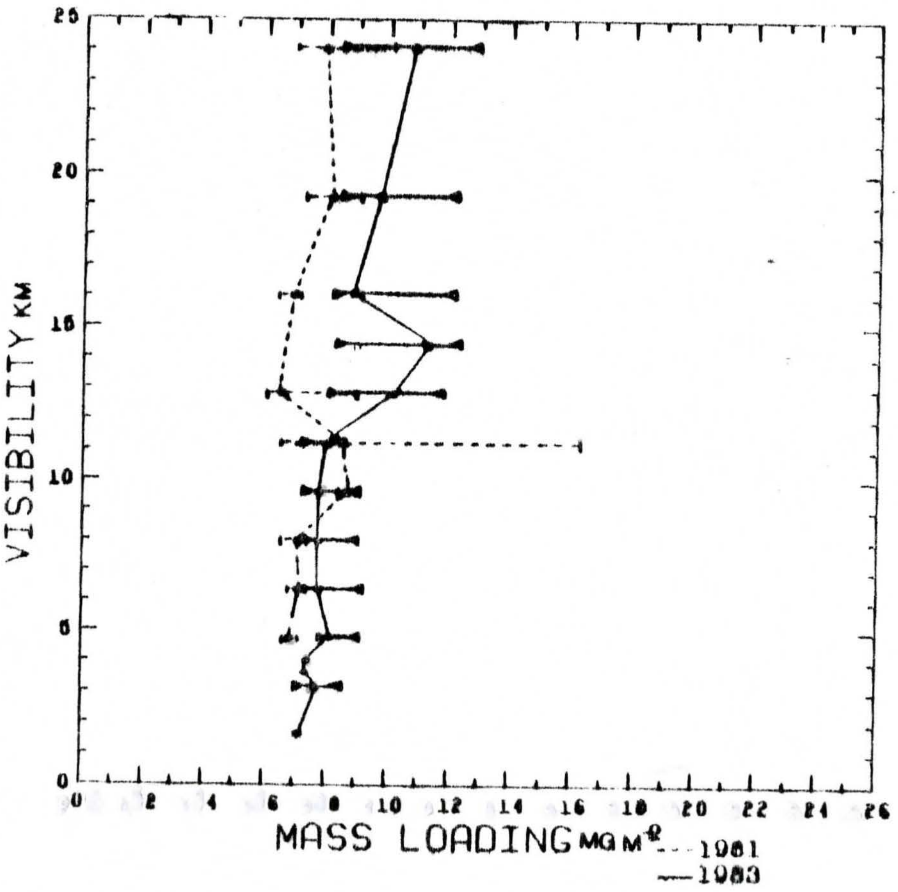

Figure 15. Correlation between visibility and mass loading, • indicate median mass loading, Quartiles indicated by horizontal bars

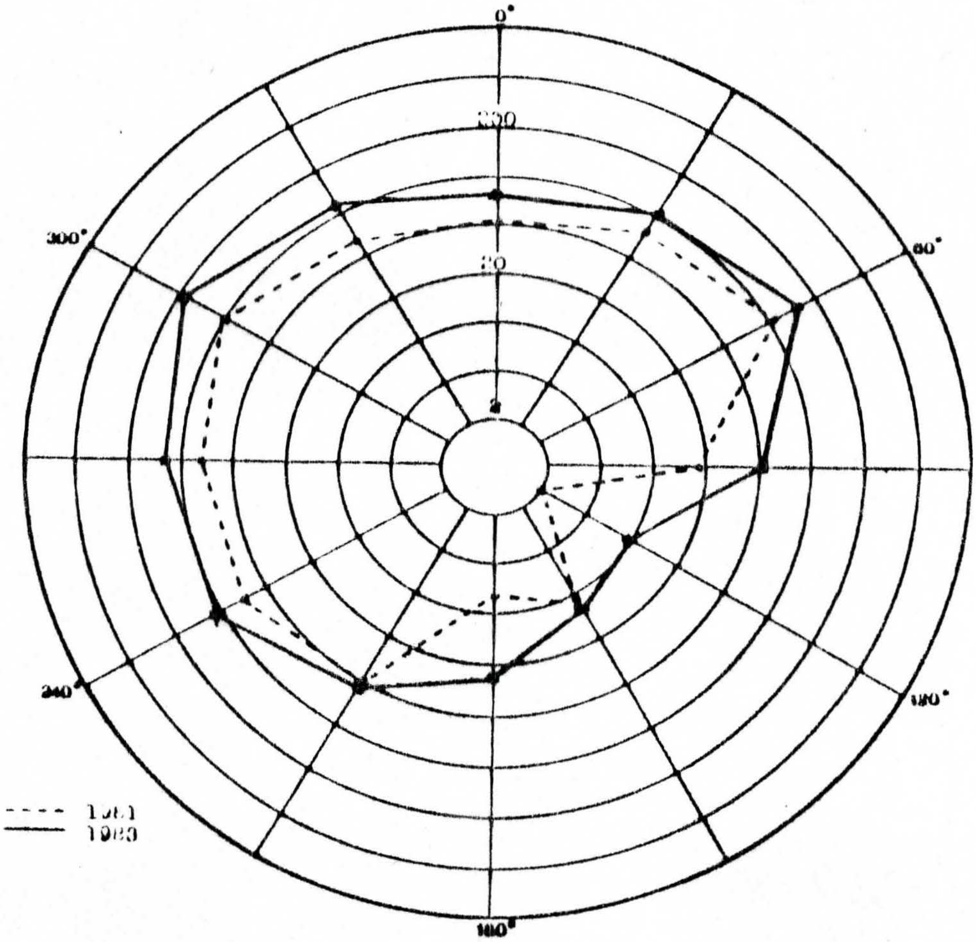

Figure 16. Number of observations from wind sectors with wind speeds greater than 2 knots.

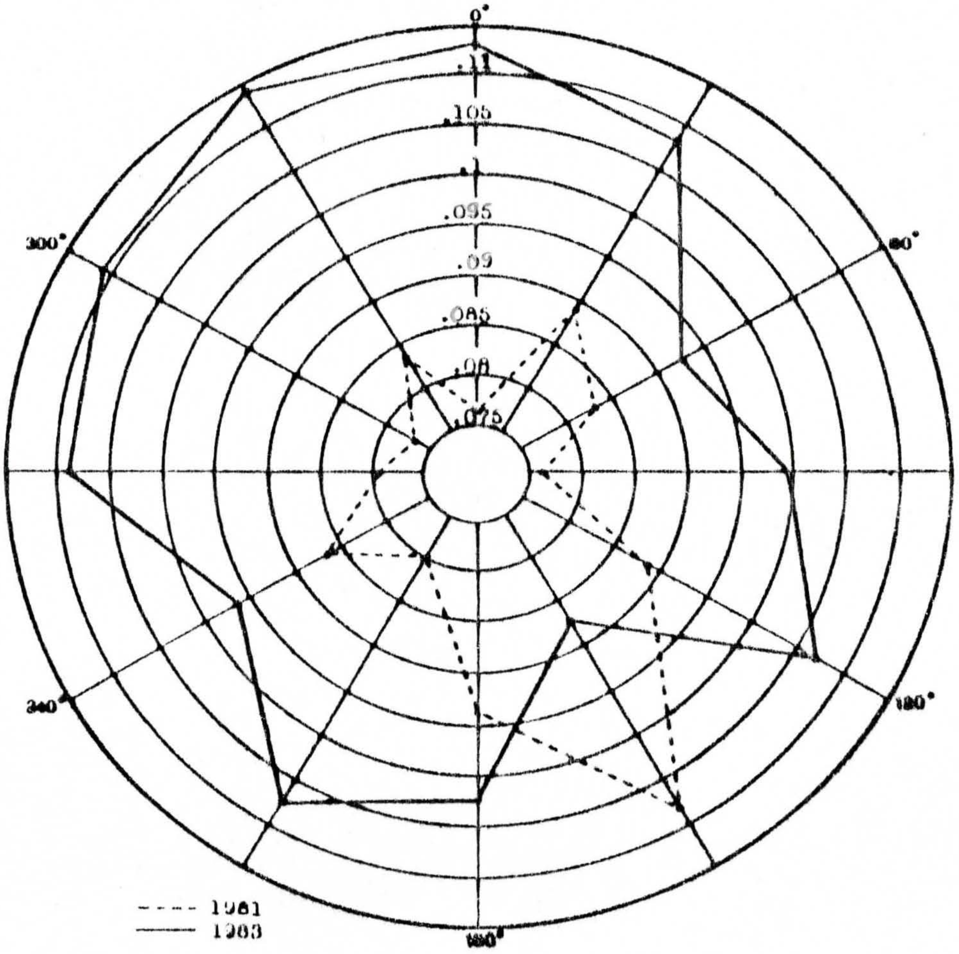

Figure 17. Variation of median aerosol mode radius (μm) with wind direction.

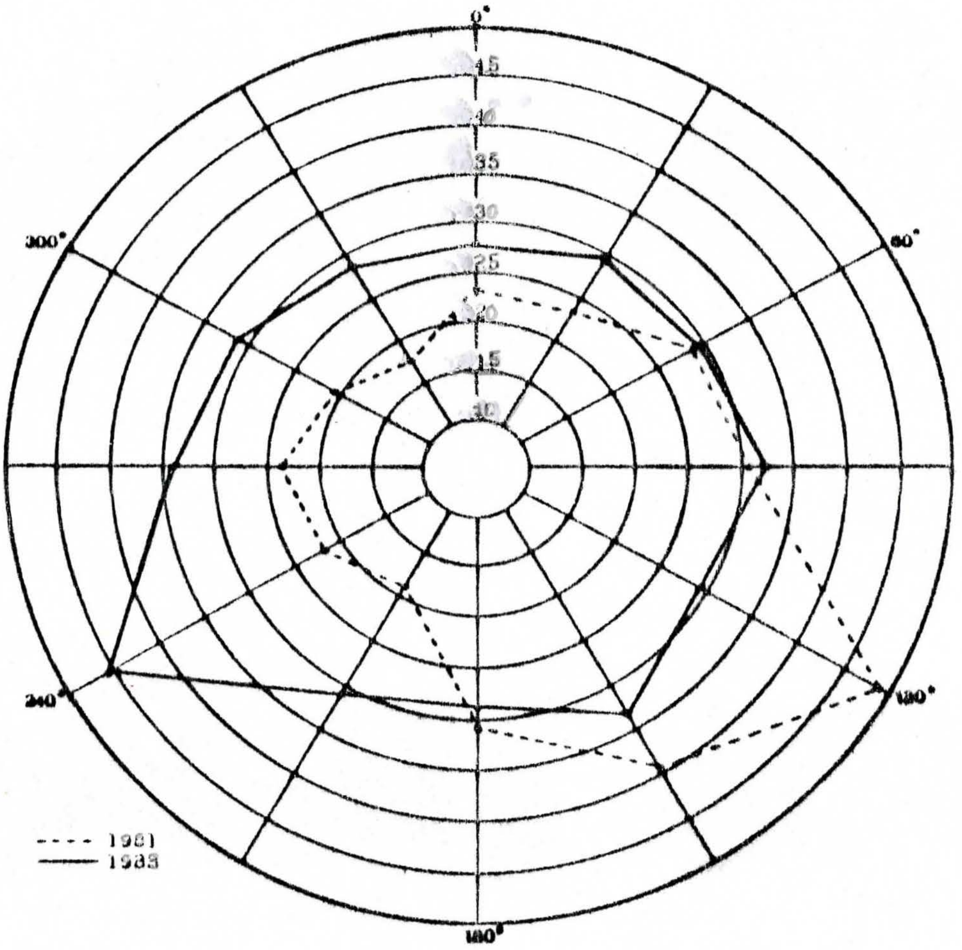

Figure 18. Variation of median aerosol mass loading (mg m^{-2}) with wind direction.

(Kaufman and Fraser, 1983; Peterson et al., 1981). In this study, neither mode radius, mass loading, nor optical depth were related to relative humidity. Surface relative humidity may not reflect conditions at higher levels.

Four days were selected to represent aerosol mode radius and mass loading values under a variety of meteorological conditions. Uncertainties in mass loading are relatively large in all cases.

On March 24, 1983 (Figure 19), light north-west winds, moderate humidity, and high visibility persisted throughout the day. Consequently, aerosol parameters showed little variation. Under north-westerly air flow, mass loading was relatively low, mode radii were large.

June 13, 1983 (Figure 20) was very polluted. Optical depths were larger than those of a Saharan dust storm (Carlson and Benjamin, 1980). Similar days have been observed in Washington D.C. (Kaufman and Fraser, 1983). Visibility was considerably reduced, light east winds, switching to south-east increased mass loading to very high levels. The hot, moist tropical airmass transported a large mass of small particles into the region.

On June 23, 1983 (Figure 21) winds were constantly from the south-east. Wind speeds increased, visibility and humidity decreased. The increased wind speed, increased the aerosol mass loading, which decreased visibility. Decreasing relative humidity may have the effect of decreasing mode radius.

The synoptic airmass changed on July 12, 1983 (Figure 22).

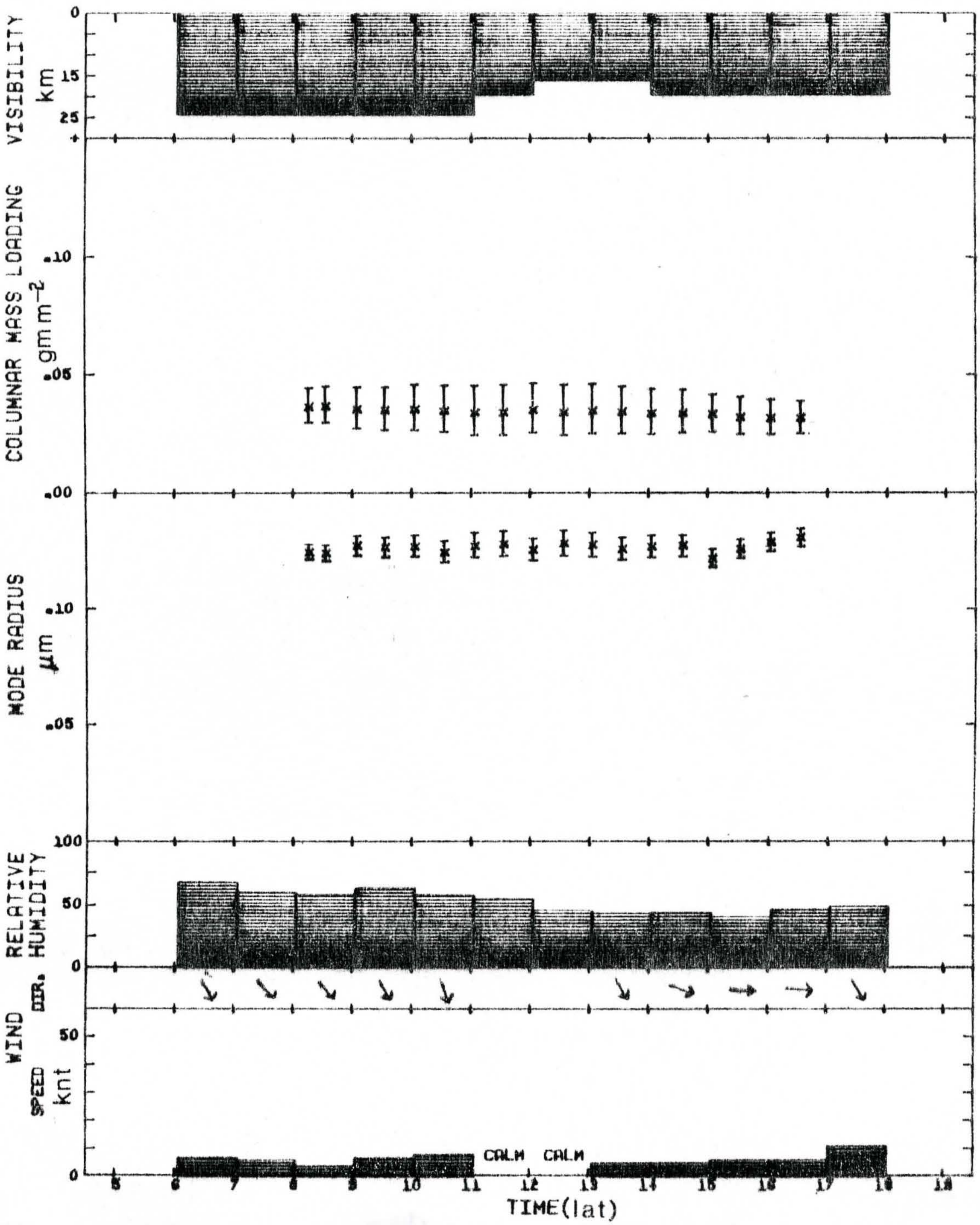

Figure 19. Diurnal variation in visibility, mode radius,mass loading,relative humidity, wind direction and speed on March 24, 1983.

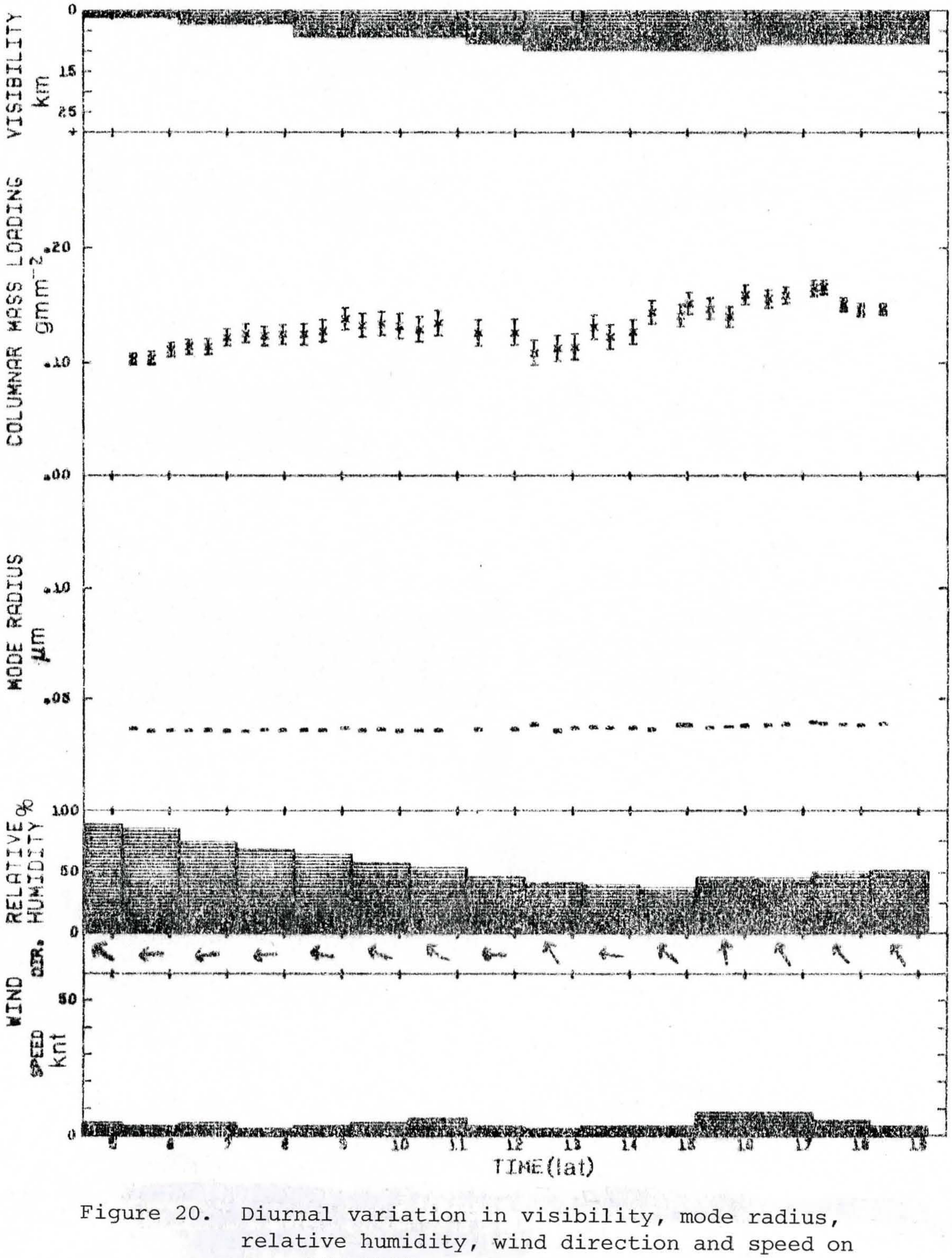

Figure 20. Diurnal variation in visibility, mode radius, relative humidity, wind direction and speed on June 13, 1983.

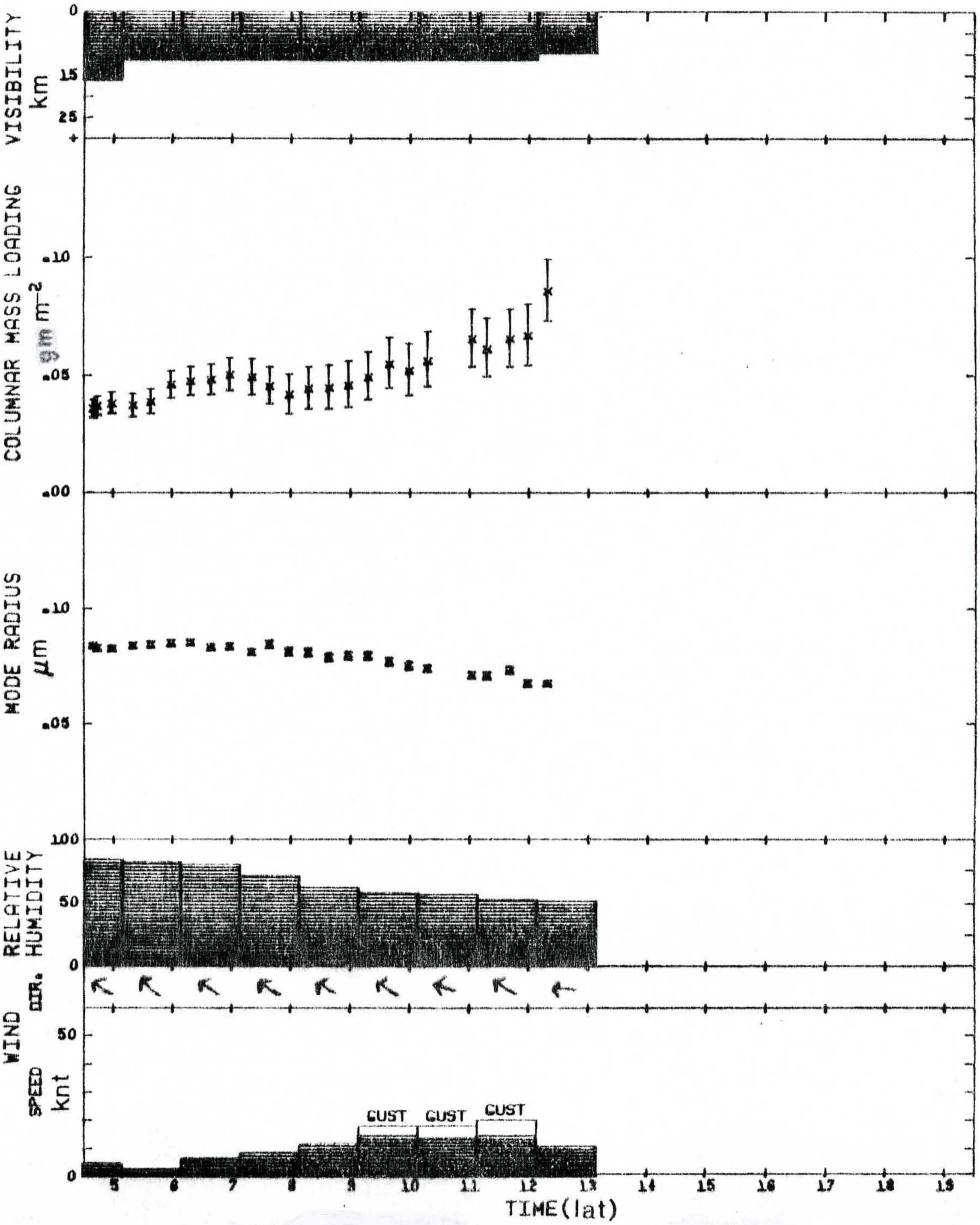

Figure 21. Diurnal variation in visibility, mode radius, mass loading, relative humidity, wind direction and speed on June 23, 1981.

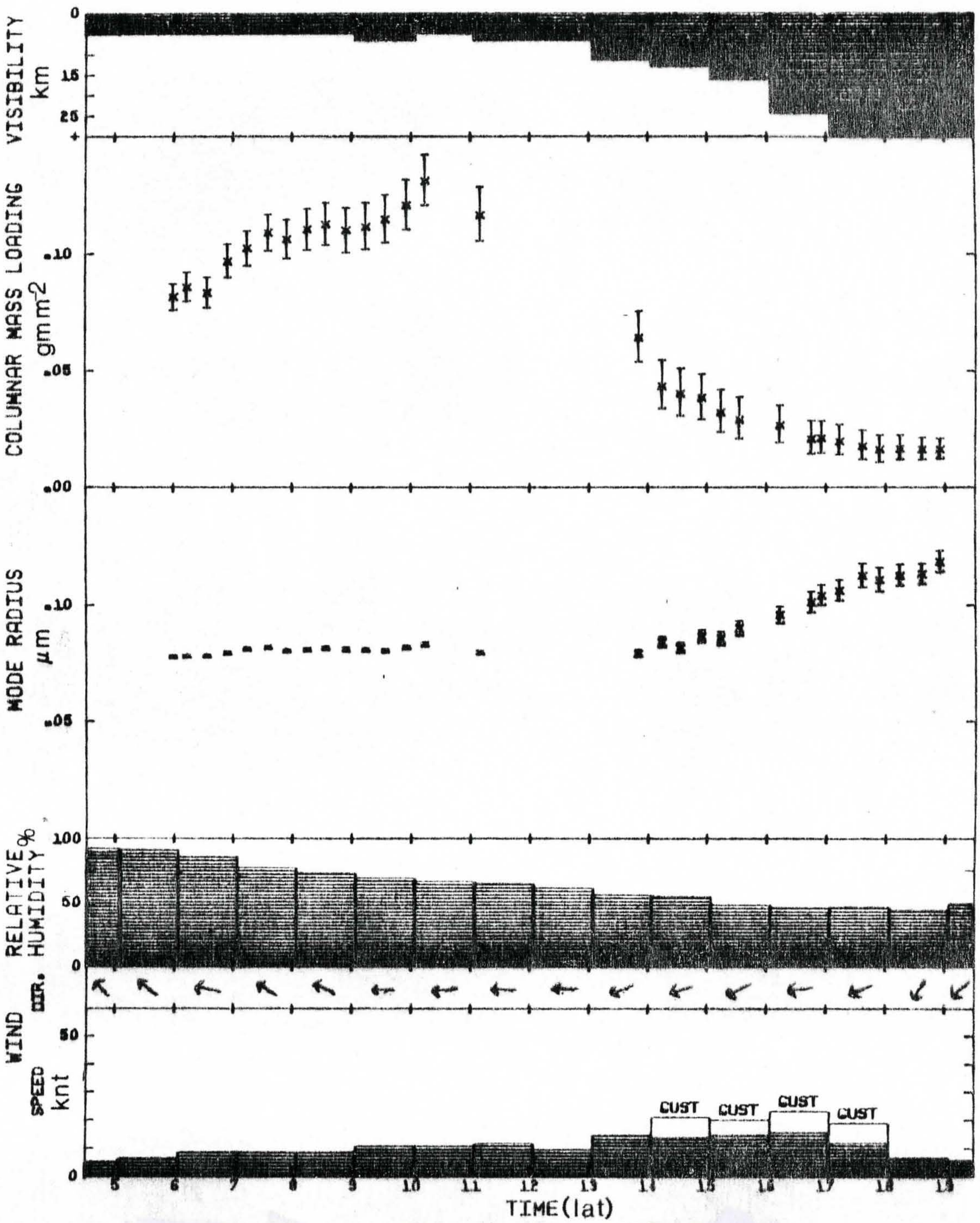

Figure 22. Diurnal variation in visibility, mode radius, mass loading, relative humidity, wind direction and speed on July 12, 1983.

Changes in wind direction, speed, and relative humidity all dramatically affected the aerosol parameters. The effect of the change from a southern to northern airmass is pronounced. A decrease in mass loading, with corresponding increases in visibility followed changes in wind direction and increased wind speed. Mode radius increased because larger stratospheric particles increased the particle size distribution.

CHAPTER FIVE

CONCLUSIONS

Aerosol optical depths in 1983 were larger by about 0.06 than aerosol optical depth in 1981 due to the eruption of El Chichón. The attenuation of direct beam radiation was not wavelength dependent. This indicates an increase in the number of large particles.

Both the size and mass of aerosol increased after the eruption. This was especially noticeable with a clean troposphere (high visibility or north-west winds). The largest size increases occurred before June, 1983, after which sizes returned towards pre-El Chichón levels. The increased particle mass however, remained constant throughout the measurement period, possibly because precipitation of larger particles was compensated by formation of new, smaller particles by gas-to-particle conversion.

Increased aerosol amount increases the planetary albedo through backscatter. Absorption by aerosol increases the temperature of the aerosol layer. Radiative convective models, using a stratospheric optical depth of 0.1, show a warming of $\sim 1^{o}C$ in the aerosol layer, and a cooling of $\sim 2^{o}C$ above the layer (Pollack and Ackermann 1983). The model predicts surface cooling over land, but the large ocean heat capacity dampens the temperature response.

Aerosol parameters varied considerably from day to day, responding primarily to meteorological conditions. Generally, northern air masses have a lower aerosol mass, while southern air masses are turbid. Radiation attenuation in very turbid air reached levels comparable to those reported for a Saharan sand storm.

The Box and Lo inversion technique was used to determine parameters of the incomplete gamma distribution given by Deirmendjian. Error in determining mass loading was large. In addition, aerosol density and refractive index had to be assumed and the effects of NO_2 were neglected.

Tropospheric aerosol distributions are probably multi-modal (Kaufman and Fraser, 1983; Whitby, 1978). Volcanic aerosol may add another mode. The inversion method used in this study accommodates only one mode. Alternative inversion methods, which accommodate several modes should be applied.

Extremely high pollution days indicate the potential importance of mankind's contribution to tropospheric aerosol loading, which may produce significant climatic perturbation. Coakley et al. (1983) showed recently that background tropospheric aerosol, which is not due to mankind's activities, may suppress global surface temperature by $2^{\circ}C$.

References

Ångström, A., 1964. The parameters of atmospheric turbidity. Tellus, 16, 64-75.

Bevington, P.R., 1969. Data Reduction and Error Analysis for the Physical Sciences. McGraw-Hill, New York, 336 p.

Box, M.A., Lo, S., 1976. Approximate determination of aerosol size distributions, J. Appl. Meteor., 15, 1068-1076.

Buck, A.L., 1981. New Equations for computing vapour pressure and Enchancement Factor, J. Appl. Meteor., 20, 1527-1532.

Carlson, K.N., Benjamin, S.G., 1980. Radiative heating rates for Saharan Dust, J. Atmos. Sci., 37, 193-213.

Coakley, J.A., Cess, R.D., Yurerich, F.B., 1983. The effect of Tropospheric Aerosols on the Earth's Radiation Budget: A Parameterization for Climate Models, J. Atmos. Sci., 40, 116-138.

Davies, J.A., 1982. Determination of Aerosol Effects and Parameters from Radiation Measurements. Report to the Atmospheric Environmental Service. McMaster University, Hamilton, 59 p.

Davies, J.A., McArthur, L.J.B., Schroeder, R., 1984. The Effect of Tropospheric and Volcanic Aerosols on Spectral Radiation Measurements. Report to the Atmospheric Environmental Service. McMaster University, Hamilton.

DeLuisi, J.J., Dutton, E.G., Coulson, K.L., DeFoor, T.E., Mendonca, B.G., 1983. On Some Radiative Features of the El Chichón Volcanic Stratospheric Dust Cloud and a Cloud of Unknown Origin Observed at Mauna Loa, J. Geophys. Res., 88, 6769-6772.

Deirmendjian, D., 1969. Electromagnetic Scattering on Spherical Polydispersions, Elsevier, New York, 290 p.

Dutton, E., DeLuisi, J., 1983. Spectral Extinction of Direct Solar Radiation by the El Chichón Cloud during December 1982, Geophys. Res. Lett., 10, 1013-1016.

Elterman L., 1968. U.V., Visible and I.R. attenuation for altitudes to 50 km. Air Froce Cambridge Research Laboratories, Environ. Res. Pap., 285, Bedford, Mass., 49 p.

Fröhlich, G., Shaw, G.E., 1980. New determination of Rayleigh Scattering in the Terrestrial Atmosphere, Appl. Opt., 19, 1753-1755.

Gradshteyn, I.S., Ryzhnik, I.M., 1975. Table of integrals, series and products, Academic Press.

Griffing, G.W., 1979. Relationship Between the Prevailing Visibility, Nephelometer Scattering Coefficient and Sunphotometer Turbidity Coefficient, Atmos. Environ., 14, 577-584.

Hänel, G., 1976. The Properties of Atmospheric Aerosol Particles as Functions of the Relative Humidity at Thermodynamic Equilibrium with the Surrounding Moist Air, Adv. Geophys., 19, 73-188.

Hofmann, D.J., Rosen, J.M., 1983. Sulfuric Acid Droplet Formation and Growth in the Stratosphere after the 1982 Eruption of El Chichón, Science, 222, 325-327.

Kaufman, Y.J., Fraser, R.S., 1983. Light Extinction by Aerosols during Summer Air Pollution, J. Appl. Meteor., 22, 1694-1706.

Kuriyan, J.G., Phillips, D.H., Willson, R.C., 1974. Determination of Optical parameters of Atmospheric particulates from Ground-based Polarimeter measurements, Quart. J. Roy. Meteorol. Soc., 100, 665-667.

Kuriyan, J.G., Sekara, Z., 1974. Scattering in liquid haze-analytic approximations, Quart. J. Roy. Meteorol. Soc., 100, 67-75.

Laulainen, N.S., Alkezweeny, A.J., Thorp, J.M., 1978. Simultaneous Aerosol Size Distribution and Turbidity Measurements over St. Louis during METROMEX 1975, J. Appl. Meteor., 17, 615-626.

Noll, K.E., Mueller, P.K., Imada, M., 1968. Visibility and Aerosol Concentration in Urban Air, Atmos. Environ., 2, 465-475.

Paltridge, G.W., Platt, C.M.R., 1976. Radiative processes in Meteorology and Climatology., Elsevier, New York, 318 p.

Peterson, J.T., Flowers, E.C., Berri, G.J., Reynolds, C.L., Rudisill, J.H., 1981. Atmospheric Turbidity over Central North Carolina, J. Appl. Meteor., 20, 229-241.

Pollack, J.B., Toon, O.B., Sagan, C., Summers, A., Baldwin, B., Van Camp, W., 1976. Volcanic Explosions and Climatic Change: A Theoretical Assessment, J. Geophys. Res., 81, 1071-1083.

Pollack, J.B., Ackerman, T.P., 1983. Possible Effects of the El Chichón Volcanic Cloud on the Radiation Budget of the Northern Tropics, Geophys. Res. Lett., 10, 1057-1060.

Pollack, J.B., Toon, O.B., Danielson, E.F., Hofmann, D.J., Rosen, J.M., 1983. The El Chichón Volcanic Cloud: An Introduction, Geophys. Res. Lett., 10, 989-992.

Prospero, J.M., Charlson, R.J., Mohnen, V., Jaenicke, R., Delany, A.C., Moyers, J., Zoller, W., Rahn, K., 1983. The Atmospheric Aerosol System: An Overview, Rev. Geophys. Space Phys., 17, 1607-1629.

Russell, P.B., Livingston, J.M., Uthe, E.E., 1979. Aerosol-Induced Albedo-Change: Measuring and Modeling of an Incident, J. Atmos. Sci., 36, 1587-1608.

Shaw, G.E., 1976. Nitrogen Dioxide-Optical Absorption in the Visible, J. Geophys. Res., 81, 5791-5792.

Shaw, G.E., Reagan, J.A., Herman, B.M., 1973. Investigations of Atmospheric Extinction using Direct Solar Radiation Measurements Made with a Multiple Wavelength Radiometer, J. Appl. Meteor., 12, 374-380.

Spinhirne, J.D., 1983. El Chichón Eruption Cloud: Latitudinal Variation of the Spectral Optical Thickness for October 1982, Geophys. Res. Let., 10, 881-884.

Stewart, K., 1982. Aerosol Effect of Spectral Direct Beam Solar Radiation at Hamilton, Ontario. B.A. Thesis, McMaster University, Department of Geography, 56 p.

Thomason, L.W., Herman, B.M., Schotland, R.M., Reagan, J.A., 1982. Extraterrestrial Solar Flux Limitations due to a Beer's Law assumption and uncertainty in Local Time, Appl. Opt., 21, 1191-1195.

van de Hulst, H.C., 1957. Light Scattering by Small Particles. John Wiley and Sons, New York, 407 p.

Whitby, K.T., 1978. Size Distribution and Physical Properties of Combustion Aerosols. Proceedings: Carbonaceous Particles in the Atmosphere. (T. Novakov ed.) Berkeley, CONF-7803101l, UC-11.